Ion channeling effects on quantum well intermixing in phosphorus-implanted InGaAsP/InGaAs/InP

D. Barba,[a] B. Salem, D. Morris, V. Aimez, and J. Beauvais
Centre de Recherche en Nanofabrication et en Nanocaractérisation, Université de Sherbrooke, Sherbrooke, Canada J1K 2R1

M. Chicoine and F. Schiettekatte
Département de Physique, Université de Montréal, Canada H3C 3J7

(Received 2 May 2005; accepted 18 July 2005; published online 7 September 2005)

Photoluminescence, time-resolved photoluminescence, and Raman characterization techniques have been used to study $In_{0.73}Ga_{0.27}As_{0.57}P_{0.43}/In_{0.53}Ga_{0.47}As/InP$ single quantum well heterostructure after 20-keV phosphorus ion implantation followed by rapid thermal annealing. The annealing process induces intermixing in the heterostructures and results in the blueshift of the quantum well peak emission. In order to investigate ion channeling effects on this band-gap tuning process, room-temperature implantations have been performed at tilt angles of 0° and 7° with respect to the sample (001)-growth axis. We show that the ion channeling increases the blueshift from 24 to 42 nm, while it reduces both the density of the nonradiative defects within the active layer and the structure disordering. These features are attributed to the nature of the damage generated by channeled ions. The band-gap increase observed in the sample implanted at 0° is consistent with the formation of a compressive strain at the barrier/quantum well interface, whose intensity is measured by Raman spectroscopy. © *2005 American Institute of Physics*. [DOI: 10.1063/1.2033143]

I. INTRODUCTION

Quantum well intermixing (QWI) based on low-energy ion implantation followed by rapid thermal annealing (RTA) is a promising technique for achieving high spatially selective band-gap tuning in III-V semiconductors.[1] Less damaging for the material than high-energy implants,[2–4] this technique has allowed Aimez *et al.* to blueshift the emission wavelength of multilayered InGaAsP/InGaAs/InP heterostructures by up to 100 nm.[5] The postgrowth process consists first in ion implantation at room temperature into a specially designed sacrificial layer, located above the quantum well (QW), and then in promoting the diffusion of the resulting defects toward the active layers, using thermal activation. During RTA, the spread of these defects enhances the mixing of atoms through the barrier/QW interface, where the local composition change modifies the band-gap energy.[6,7] Compared to the impurity-free methods, using dielectric encapsulants[8,9] or the diffusion of grown-in defects,[10] this technique offers a better control of the damage profile within the target material, since the density and the spatial distribution of the defects induced by ion implantation can be set directly with appropriate fluence and ion-beam energy.[4]

In InGaAs/InP and InGaAsP/InP heterostructures, the QWI efficiency is mediated by the diffusion of both anion and cation sublattices, whose concentration profiles can be determined by means of secondary-ion-mass spectroscopy[11] or scanning tunneling microscopy.[12] Although some recent works give a greater importance to the enhanced group-V sublattice diffusion,[11–13] these studies have not allowed the authors to describe the QWI process by a single and unique mechanism in InP-based materials. The optical measurements show that the degree of intermixing depends on the sample composition and the nature of the disorder introduced in the structure.

It has also been established that QWI is sensitive to the presence of mechanical stress in the active layer.[14] Such strain modifies the electron confinement by notably splitting the heavy hole (hh)-light hole (lh) band degeneracy. Direct consequences on the optical properties have been investigated by luminescence and Raman experiments, which show that a biaxial compressive or tensile strain enhances or reduces the band-gap increase, respectively.[14,15]

In this work, we used photoluminescence (PL), time-resolved photoluminescence (TRPL), and Raman spectroscopy to characterize thermal-annealed single InGaAs quantum well embedded between InGaAsP barriers, after 20-keV phosphorus implantations carried out with tilt angles of 7° and 0°. These three complementary techniques enabled us to examine the optical properties of the implanted materials as a function of the structural changes induced by negligible and effective ion channeling.[16] First, we show that the ion channeling enhances simultaneously the blueshift and the lifetime of photocarriers in the active layer. Then, we used Raman investigations of Ga–As bonding vibrations to characterize the disordered InGaAs QW layer. The significant improvement of the band-gap tuning process is discussed by considering the damage profile in the ion-implanted samples, using Monte Carlo simulations. We argue that the increase of the blueshift observed in the material implanted at 0° is consistent with the compressive strain formation at the barrier/QW interface, whose intensity is deduced from Raman measurements.

[a]Electronic mail: dbarba@physique.usherb.ca

 © 2005 American Institute of Physics

Downloaded 20 Dec 2006 to 132.204.95.70. Redistribution subject to AIP license or copyright, see http://jap.aip.org/jap/copyright.jsp

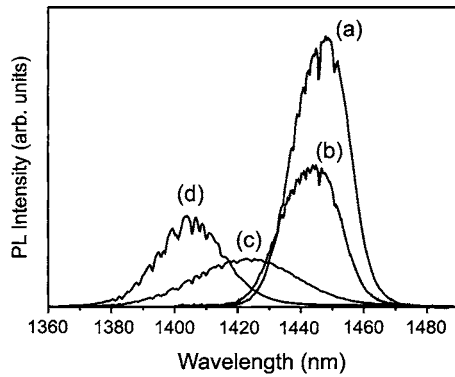

FIG. 1. PL measurements obtained at $T=20$ K in as-grown material (a), unimplanted + annealed sample (b), and annealed samples after P^+ implantations performed at $\theta=7°$ (c) and $\theta=0°$ (d), respectively.

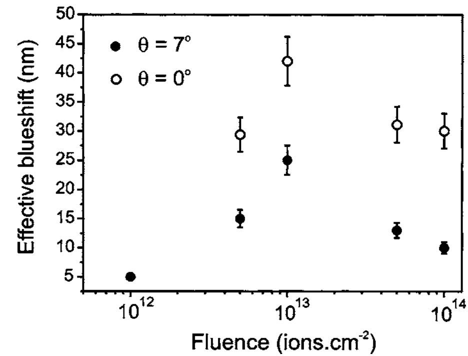

FIG. 2. Effective blueshift measured with respect to the unimplanted sample after RTA at 660 °C during 60 s, as a function of the ion implantation dose. (●) denotes implanted material at 20 keV with $\theta=7°$, and (○) with $\theta=0°$.

II. EXPERIMENTS

The samples were grown by metal-organic chemical-vapor deposition on (001)-oriented InP wafer. A first 1-μm buffer layer of InP was grown on an Fe-doped InP substrate, followed by an 80-nm $In_{0.85}Ga_{0.15}As_{0.32}P_{0.68}$ ($Q=1.10$ μm) buffer, and a 50-nm-thick $In_{0.79}Ga_{0.21}As_{0.45}P_{0.55}$ ($Q=1.18$ μm) layer. The quantum well consists of 5.5-nm $In_{0.53}Ga_{0.47}As$ layer sandwiched between 12 and 40-nm-thick $In_{0.73}Ga_{0.27}As_{0.57}P_{0.43}$ ($Q=1.28$ μm) barriers, and the structure was capped with a 70-nm InP cladding layer. The concentrations of ternary and quaternary alloys have been adjusted to ensure lattice matching[17] so that the QW is nominally unstrained.

Ion implantations were carried out at $T=20$ °C using an ion-beam energy of 20 keV. Phosphorus ions were implanted at tilt angles set to 0° and 7° with a ±1° accuracy, for fluences varying between 5×10^{12} and 10^{14} ions cm^{-2}. The annealing temperature of 660 °C was chosen to obtain maximum effective blueshifts. RTA was performed for 60 s under N_2/H_2 mixture atmosphere using a JetFirst rapid thermal processor. In order to minimize outgassing effects during the annealing, samples were laid face down on the silicon susceptor in the RTA, and the back side of the samples is covered by an InP cap.

Photoluminescence spectra were recorded at 20 K, using the 905-nm line of a near-infrared laser diode and a closed-cycle refrigerator system. Time-resolved photoluminescence measurements were performed at 77 K using a mode-locked Ti:sapphire laser (100 fs, 82–750 nm) for excitation, an up-conversion technique with subpicosecond temporal resolution, and a GaAs photomultiplier tube for detection. Power excitation densities were varied between 2 and 200 W cm^{-2}. Micro-Raman studies with 1-cm^{-1} resolution were carried out at 10 K in the $z(xy)\bar{z}$ backscattering geometry by means of a LABRAM-800 confocal system equipped with a nitrogen-cooled charge-coupled device (CCD) detector, a 50× microscope lens, and a continuous-flow temperature-regulated helium cryostat. A 514.5-nm Ar laser line polarized parallel to the sample surface and focused on a diameter spot of a few microns was used for excitation. To reduce the contribution of surface defects to the experimental data, the micro-Raman measurements were obtained with 1-mm confocal hole.

III. RESULTS

A. Luminescence measurements

PL spectra of as-grown, annealed, and both implanted and annealed samples are presented in Fig. 1. Blueshifts of 2, 24, and 42 nm measured with respect to the as-grown sample were obtained after RTA for the unimplanted material, the sample implanted at $\theta=7°$, and the sample implanted at $\theta=0°$, respectively. Similar PL shifts (not shown) were observed after sacrificial InP layer removal, or RTA performed during 120 s. In any case, a blueshift improvement of about 50% as well as an increase of the PL emission was systematically reported for the ion-implanted samples at 0°. Figure 2 shows that the effective blueshift increases continuously with the increasing amount of defects introduced into the structure for ion implantation doses ranging from 10^{12} to 10^{13} ions cm^{-2}. The band-gap tuning reaches a maximum value at a fluence of 10^{13} ions cm^{-2}, which corresponds to the amorphization threshold of InP for room temperature implantation.[18]

In Fig. 3, we present the temporal evolution of the PL signals detected at the maximum of each spectrum shown in Fig. 1. The effective rise time ($\tau_{\rm rise}$) and decay time ($\tau_{\rm decay}$)

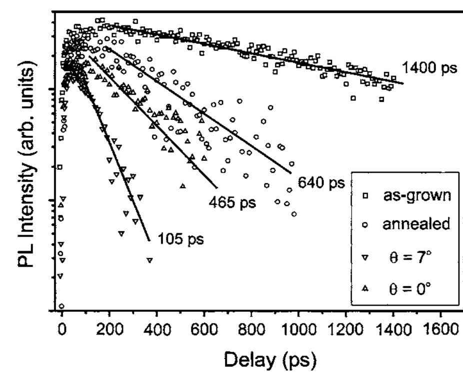

FIG. 3. Time-resolved photoluminescence spectra measured at 77 K, with corresponding decay times extracted from the reported curve slopes.

Downloaded 20 Dec 2006 to 132.204.95.70. Redistribution subject to AIP license or copyright, see http://jap.aip.org/jap/copyright.jsp

TABLE I. PL capture time (τ_{rise}) and decay time (τ_{decay}) measured for the $In_{0.53}Ga_{0.47}As$ QW.

Sample	τ_{rise} (ps)	τ_{decay} (ps)
As-grown	22±2	1400±35
Annealed	19±2	640±15
Implanted at 7° and annealed	13±2	105±10
Implanted at 0° and annealed	14±2	465±10

were determined by fitting the experimental data with the following solution of the three-level model for the photocarrier population rate equations:

$$I_{PL}(t) = \frac{a(e^{-t/\tau_{rise}} - e^{-t/\tau_{decay}})}{\tau_{decay} - \tau_{rise}}. \quad (1)$$

The effective rise time corresponds to the QW capture/relaxation time. It is mainly limited by the carrier transport within the InP and the InGaAsP layers. On the other hand, the effective decay time corresponds to the carrier recombination time. For the ion-implanted materials, this decay time is limited by nonradiative recombination of carriers excited in the QW and the barriers. The fitting values obtained for the rise and decay times are given in Table I.

In agreement with previous TRPL investigations of InGaAs quantum wells,[19] we measured a smaller PL rise time in the ion-implanted samples. This enhanced carrier capture efficiency might result from an induced internal electric field associated with the concentration gradient at the barrier/QW interface. We observed an order of magnitude variation of the decay time in the studied samples. Smaller decay times reveal a higher density of nonradiative recombination centers within the QW after ion implantation and annealing. Therefore, the decay time of 105 ps measured in the sample implanted at 7° indicates that its active layer is more disordered than in the material implanted at 0°. Note that the smallest decay time (see Table I), the broadest emission band, and the weakest PL signal [see Fig. 1(c)] were simultaneously obtained for the sample implanted at 7°, thus confirming the correlation existing between the spatial fluctuation of the optical confinement and the presence of residual defects within the QW. It is finally important to outline that the larger PL blueshift is not recorded in the sample where the highest degree of disorder was observed.

B. Raman scattering

The maximum penetration depth of the 514.5-nm laser line is approximately 120 nm. In order to probe the QW InGaAs layer, which is located 110 nm below the surface of the as-grown material, the 70-nm InP cladding has been removed by selective etching using a H_3PO_4:HCl (3:1) mixture. Figure 4 shows the Raman spectra obtained at $T = 300$ K for the as-grown material before (a) and after (b) etching. This figure confirms the four-mode behavior of InGaAs and InGaAsP layers. The peaks observed between 210 and 280 cm^{-1} are attributed to the longitudinal-optical (LO) In–As and Ga–As bond vibrations, and those observed between 300 and 350 cm^{-1} correspond to the In–P and Ga–P LO vibrations. The extinction of the strong peak at 345 cm^{-1} on Fig. 4(b), associated with the InP Raman signature, gives evidence of the complete cladding removal. This remark is corroborated by the simultaneous observation of an additional mode around 270 cm^{-1}, which is attributed to the $In_{0.53}Ga_{0.47}As$ well. We also notice at 145 cm^{-1} the disorder-activated longitudinal acoustic phonon (DALA),[20,21] and we observe multiphonons (2-ph) between 600 and 700 cm^{-1}, connected with a second-order combination of LO and TO modes.[21] The weak signal above 300 cm^{-1} [Fig. 4(b)] forces us to limit our Raman study to the 210–280-cm^{-1} spectral range.

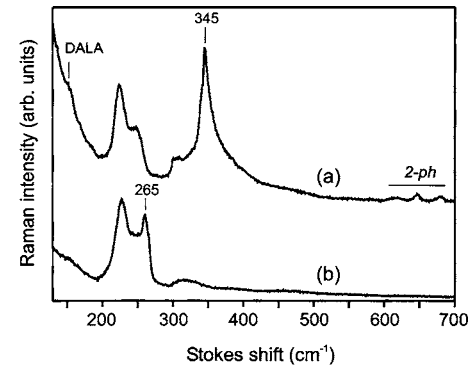

FIG. 4. Room-temperature $z(xy)\bar{z}$ Raman spectra of as-grown sample before (a) and after (b) InP layer removal.

In Fig. 5, the solid line refers to the fit of the data by four Gaussians (dashed lines). For $z(xy)\bar{z}$ optical configuration, only the LO modes are dipole-allowed. Using the previous Raman reports available for $In_{1-x}Ga_xAs_yP_{1-y}$/InP systems,[20–24] the bands observed around 230 (mode 1), 255 (mode 2), 265 (mode 3), and 270 cm^{-1} (mode 4) are assigned as the following: modes 1 and 3 are attributed to the InAs(LO)-like and GaAs(LO)-like phonons coming from barriers, whereas modes 2 and 4 correspond to InAs(LO)-like and GaAs(LO)-like phonons coming from the QW, respectively.

Due to the overlap of the Raman peaks between 210 and 280 cm^{-1}, as well as the possible contribution of forbidden TO components to the spectra below 250 cm^{-1}, the quantitative analysis is restricted to the GaAs(LO) phonon (mode 4). We observe this phonon at 270 cm^{-1} in both the reference and annealed materials, and at 267 and 269 cm^{-1} in the samples implanted at 7° and 0°, respectively. In Figs. 5(c) and 5(d), the Raman intensity lowering of the GaAs(LO) mode and its apparent bandwidth broadening both indicate the breakdown of several Ga–As bonds in the implanted materials. Such a reduction is less significant for the sample implanted at 0° than for the one implanted at 7°. This reveals a higher structural disordering for the ion-implanted sample at 7°.

The measured energy of 270 cm^{-1} (ω_0) from the reference material in Fig. 5(a) is very close to the value reported for unstrained $In_{0.53}Ga_{0.47}As$ layer.[21,22] We obtain Raman downshifts ($\Delta\Omega_{LO}$) of 3 cm^{-1} in the ion-implanted sample at 7° and 1 cm^{-1} in the sample implanted at 0°, with respect to ω_0. These spectral shifts give evidence of the atomic species exchange through the InGaAsP/InGaAs interface.[15,24] The percentage of arsenic leaving the QW during the RTA can be

Downloaded 20 Dec 2006 to 132.204.95.70. Redistribution subject to AIP license or copyright, see http://jap.aip.org/jap/copyright.jsp

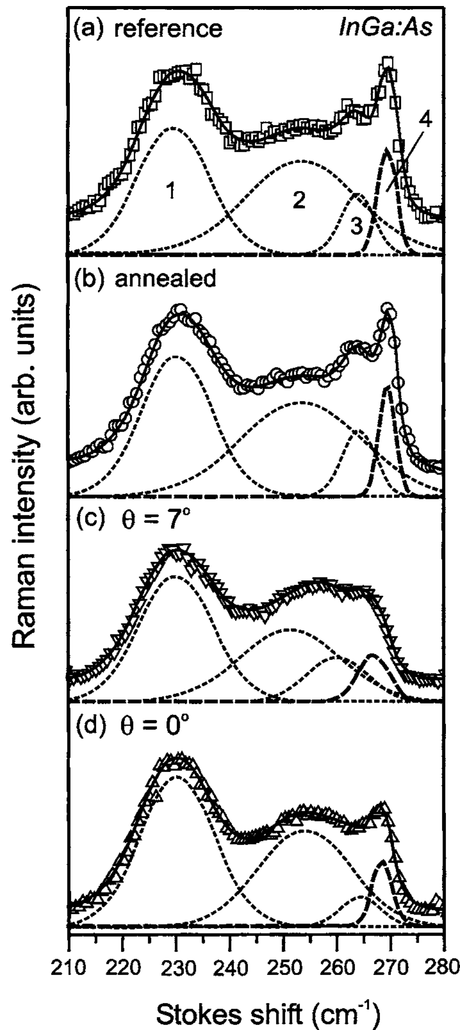

FIG. 5. $z(xy)\bar{z}$ Raman spectra obtained at $T=10$ K after InP layer removal: (a) reference material, (b) annealed sample, (c) implanted at $\theta=7°$ and annealed sample, and (d) implanted at $\theta=0°$ and annealed sample.

evaluated from the Raman measurements using the empirical relation found by Peyre *et al.* for lattice-matched InGaAsP/InGaAs systems,[24]

$$\frac{\Delta y}{\Delta \Omega_{\mathrm{LO}}} = 4 \times 10^{-2} \text{ (cm)}. \quad (2)$$

If we assume that the intermixed InGaAs active layer remains unstrained after ion implantation followed by thermal annealing, the Raman downshifts of GaAs(LO) phonons correspond to an arsenic content lowering of 12.4% and 4.8% in the ion-implanted samples at 7° and 0°, respectively.

IV. DISCUSSION

For 20-keV phosphorus ion implantation in an InP layer at 7°, an average projected range of about 25 nm is given by SRIM Monte Carlo simulations.[25] In the absence of ion channeling, whose effects are not taken into account by the SRIM code, the damage profile resulting from ion implants does not reach the InGaAsP upper barrier located at 70 nm below the sample surface. Therefore, we can assume that in the sample implanted at 7° the QWI mechanism is solely mediated by the spread of point defects generated within the InP sacrificial layer through the InGaAs active layer. In this material, the defect distribution is also more concentrated in the vicinity of the sample surface. This may result locally in the formation of defect complexes or aggregates with high diffusion activation energy. Since the complete removal of these extended defects during the InP selective etching does not affect the PL spectra, their contribution to the optical properties of the implanted materials are negligible.

For an implantation performed at 0°, the ion channeling tail leads to an extension of the damage distribution through the active layer, so that defects are directly produced in the QW. Indeed, crystal-TRIM (Ref. 26) Monte Carlo simulations performed for 20-keV phosphorus ions penetrating into a Si target reveal that the implantation depth for a normal incidence is about three times larger than for an implantation at $\theta=7°$. Moreover, the calculations show that the amount of defects generated in the first 110 nm of the target material is twice higher for the sample implanted at 7° than for the sample implanted at $\theta=0°$. This feature is related to the fact that the channeled ions transfer lower recoil energies to the target atoms,[16] since the energy of incident ions is mainly lost by electron stopping rather than by nuclear collisions. This could also lead to the creation of deep point defects, which affect the thermal stability of the InGaAsP/InGaAs system. On the other hand, the dilution of defects within the sample implanted at 0° favors its structural restoration during the RTA.

Since the PL shifts reported in Fig. 1 do not change for a longer annealing time, we can assume that the majority of defects contributing to the band-gap tuning have diffused through the active layer in the first 60 s of the thermal annealing. In the sample implanted at 0°, where the highest band-gap increase was observed, both the TRPL and the Raman measurements indicate that the intermixed active layer is less disordered than in the implanted sample at 7°. Such a result is in agreement with the fact that fewer defects were generated in a larger volume during the ion implantation at 0°. Nevertheless, the blueshift improvement we have systematically observed in the samples implanted at 0° on Fig. 2 indicated that the degree of intermixing does not only depend on the number of defects involved in the QWI process. This shows the occurrence of a different QWI mechanism in these samples, which is connected with the nature of the damage produced by ion channeling. Therefore, the 4.8% degree of intermixing obtained for the sample implanted at 0° from Eq. (2) is inappropriate to explain its effective blueshift of 40 nm in Fig 1(d). This underestimation may come from an energy compensation of the GaAs(LO) phonon downshift observed in Fig. 5(d). Similar features have been previously reported for stressed InGaAs/InP systems,[21,22] where the spectral shift to higher energy is associated with a compressive strain formation in the InGaAs layer.[15] The origin of this strain could be due to an excess of interstitial-type defects within the ion-implanted sample at 0°, resulting from channeled ion implantation.[27] In the next two paragraphs, we examine the effects such a compressive strain would involve on the PL blueshift. We show that the band-gap increase induced by this strain agrees with the blueshift improvement obtained for the sample implanted at 0°.

Downloaded 20 Dec 2006 to 132.204.95.70. Redistribution subject to AIP license or copyright, see http://jap.aip.org/jap/copyright.jsp

TABLE II. Parameters used in Eqs. (3)–(5).

Parameter	Symbol	Unit	$In_{0.53}Ga_{0.47}As$
As-grown GaAs(LO) phonon energy	ω_0	cm^{-1}	270
Phonon deformation potential	p	10^4 cm^{-2}	−8.04
Phonon deformation potential	q	10^4 cm^{-2}	−0.12
Elastic compliance constant	S_{11}	10^{-12} dyn^{-1} cm^2	1.58
Elastic compliance constant	S_{12}	10^{-12} dyn^{-1} cm^2	0.52
Elastic stiffness constant	C_{11}	10^{11} dyn cm^{-2}	9.99
Elastic stiffness constant	C_{12}	10^{11} dyn cm^{-2}	4.93
Hydrostatic deformation for *cb*	a'	eV	5.37
Hydrostatic deformation for *vb*	a	eV	2.59
Shear deformation potential for *vb*	b	eV	−1.75

The biaxial stress component (ϵ) associated with a Raman energy shift ($\Delta\omega$) of about 2 cm^{-1} can be obtained from the relation established by Cerdeira *et al.*[28] for a zinc-blende structure,

$$\Delta\omega = \frac{\epsilon}{3\omega_0}[(p+2q)(S_{11}+2S_{12})-(p-q)(S_{11}-S_{12})], \quad (3)$$

where $\omega_0=270\ cm^{-1}$ is the wave number of the $\vec{k}=0$ GaAs(LO) phonon, p and q are the optical phonon deformation parameters, and S_{11} and S_{12} are the elastic compliance constants. For $In_{0.53}Ga_{0.47}$, these parameters are determined by linear interpolation of the data available for InAs and GaAs. Using the values reported in Table II, the $\Delta\omega = 2.0\pm0.5\ cm^{-1}$ Raman shift measured in Figs. 5(c) and 5(d) corresponds to an in-plane compressive strain: $\epsilon = 0.07\% \pm 0.01\%$.

The band-gap increase associated with the strain effects is given by the energy corrections in the conduction (ΔE_c) band and the heavy-hole valence band (ΔE_{hh}),[15] namely,

$$\Delta E_c = 2a'\left(\frac{C_{11}-C_{12}}{C_{11}}\right)\epsilon, \quad (4)$$

$$\Delta E_{hh} = \left(2a\frac{C_{11}-C_{12}}{C_{11}} + b\frac{C_{11}+2C_{12}}{C_{11}}\right)\epsilon, \quad (5)$$

where the deformation parameters a', a, and b, as well as the elastic stiffness constants C_{11} and C_{12}, are reported in Table II. Using these relations, the energy shift induced by a compressive strain $\epsilon=0.07\%$ is 11 ± 1 meV, which corresponds to a blueshift increase of 20 nm. This latter value is consistent with the data obtained from Fig. 1(d).

V. CONCLUSION

We have studied InGaAsP/InGaAs/InP single quantum well heterostructures after 20-keV phosphorus implantations performed with tilt angles set to 0° and 7° followed by rapid thermal annealing. Photoluminescence and Raman studies show a significant improvement of the band-gap tuning process in the sample implanted at 0°. In this material, time-resolved PL and Raman measurements also indicate a lower disordering of the InGaAs active layer, where both the lifetime of photocarriers and the Raman intensity of the GaAs(LO) phonon increase. We associate these features to the ion channeling effects, which lower the damaging of the upper layers and expand the defect distribution through the active layer. The blueshift increase reported for the ion-implanted sample at 0° is quantitatively consistent with the formation of a compressive strain at the barrier/QW interface. The origin of this strain may be related to the nature and the spatial distribution of defects induced by the ion channeling.

ACKNOWLEDGMENTS

This work was supported by Nano-Québec, the Fonds de Recherche sur la Nature et les Technologies du Québec, and the Natural Sciences and Engineering Research Council of Canada. The authors would like to thank Laurent Isnard and Richard Arès of the Institut des Matériaux et des Systèmes Intelligents for complementary x-ray-diffraction analysis. We are also grateful to Professor Serge Jandl of the University of Sherbrooke for providing us access to the micro-Raman set up.

[1]M. Paquette, J. Beauvais, J. Beerens, P. J. Poole, S. Charbonneau, C. J. Miner, and C. Blaauw, Appl. Phys. Lett. **71**, 3749 (1997).
[2]S. Charbonneau, P. J. Poole, Y. Feng, G. C. Aers, M. Dion, M. Davies, R. D. Goldberg, and I. V. Mitchell, Appl. Phys. Lett. **67**, 2954 (1995).
[3]P. G. Piva *et al.*, Appl. Phys. Lett. **72**, 1599 (1998).
[4]P. J. Poole, S. Charbonneau, G. C. Aers, T. E. Jackman, M. Buchanan, M. Dion, R. D. Goldberg, and I. V. Mitchel, J. Appl. Phys. **78**, 2367 (1995).
[5]V. Aimez, J. Beauvais, J. Beerens, S. L. Ng, and B. S. Ooi, Appl. Phys. Lett. **79**, 3582 (2001).
[6]J. H. Marsh, Semicond. Sci. Technol. **8**, 1136 (1993).
[7]K. Mukai, M. Sugawara, and S. Yamazaki, Phys. Rev. B **50**, 2273 (1994).
[8]S.-W. Ryu, B.-D. Choe, and W. G. Jeong, Appl. Phys. Lett. **71**, 1670 (1997).
[9]J. S. Yu, Y. T. Lee, and H. Lim, J. Appl. Phys. **88**, 5720 (2000).
[10]J. E. Haysom, G. C. Aers, S. Raymond, and P. J. Poole, J. Appl. Phys. **88**, 3090 (2000).
[11]J. H. Teng *et al.*, J. Appl. Phys. **92**, 4330 (2002).
[12]H. Chen, R. M. Feenstra, P. G. Piva, R. D. Golberg, I. V. Mitchell, G. C. Aers, P. J. Poole, and S. Charbonneau, Appl. Phys. Lett. **75**, 79 (1999).
[13]J. E. Haysom, P. J. Poole, R. L. Williams, S. Raymond, and G. C. Aers, Solid State Commun. **116**, 187 (2000).
[14]J. Micallef, E. Herbert Li, and L. Weiss, J. Appl. Phys. **73**, 7524 (1993).
[15]S. C. Jain, M. Willander, and H. Maes, Semicond. Sci. Technol. **11**, 641 (1996).
[16]P. D. Townsend, J. C. Kelly, N. E. W. Hartley, *Ion Implantation, Sputtering and Their Applications* (Academic, London, 1976).
[17]S. Adachi, J. Appl. Phys. **53**, 8775 (1982).
[18]E. Wendler, B. Breeger, Ch. Schubert, and W. Wesch, Nucl. Instrum. Methods Phys. Res. B **147**, 155 (1999).
[19]L. V. Dao, M. B. Johnston, M. Gal, L. Fu, H. H. Tan, and C. Jagadish, Appl. Phys. Lett. **73**, 3408 (1998).
[20]R. K. Soni, S. C. Abbi, K. P. Jain, M. Balkanski, S. Slempkes, and J. L. Benchimol, J. Appl. Phys. **59**, 2184 (1986).
[21]Z. C. Feng, A. A. Allerman, P. A. Barnes, and S. Perkowitz, Appl. Phys. Lett. **60**, 1848 (1992).
[22]M. J. L. S. Haines, B. C. Cavenett, and S. T. Davey, Appl. Phys. Lett. **55**, 849 (1989).
[23]T. Sugiura, N. Hase, Y. Iguchi, and N. Sawaki, Jpn. J. Appl. Phys., Part 1 **38**, 996 (1999).
[24]H. Peyre, F. Alsina, J. Camassel, J. Pascual, and R. W. Glew, J. Appl. Phys. **73**, 3760 (1993).
[25]J. F. Ziegler, J. P. Biersack, and U. Littmark, *The Stopping and Ion Range of Ions in Matter* (Pergamon, New York, 1985).
[26]M. Posselt, Radiat. Eff. Defects Solids **130/131**, 87 (1994).
[27]S. L. Ellingboe and M. C. Ridgway, Nucl. Instrum. Methods Phys. Res. B **127/128**, 90 (1997).
[28]F. Cerdeira, C. J. Buchenauer, F. H. Pollak, and M. Cardona, Phys. Rev. B **5**, 580 (1972).

Downloaded 20 Dec 2006 to 132.204.95.70. Redistribution subject to AIP license or copyright, see http://jap.aip.org/jap/copyright.jsp